ACADEMIC PRESS

Available online at www.sciencedirect.com
SCIENCE DIRECT®

Journal of Catalysis 217 (2003) 245–252

JOURNAL OF CATALYSIS

www.elsevier.com/locate/jcat

Preparation and characterisation of a stable Rh catalyst for the partial oxidation of methane

F. Basile,[a,*] G. Fornasari,[a] M. Gazzano,[b] A. Kiennemann,[c] and A. Vaccari [a]

[a] *Dipartimento di Chimica Industriale e dei Materiali, Università di Bologna, Viale Risorgimento 4, 40131 Bologna, Italy*
[b] *CSFM/CNR, Via Selmi, 2, 40126 Bologna, Italy*
[c] *ECPM, LERCSI, 25, Rue Becquerel, 67087 Strasbourg Cedex 2, France*

Received 7 January 2002; revised 23 September 2002; accepted 23 September 2002

Abstract

A Rh catalyst (Rh/Al/Mg 5/24/71 a.r.), able to ensure high stability under severe reaction conditions, was obtained via a hydrotalcite-type precursor. The structure of the materials and the Rh position were thoroughly studied at each step of the preparation, from the precipitation to the final catalyst. The formation of an oxide solid solution of Rh, Mg, and Al was found by X-ray and neutron diffraction using Rietveld analysis. The formation of Rh dissolved in a Mg and Al matrix is responsible for the highly dispersed and active Rh catalyst obtained after reduction. The stability of the Rh on the surface after 100 h of time on stream was shown by determining the dispersion of the Rh before and after reaction (using HRTEM) and demonstrating the unchanged particle size distribution.

Keywords: Methane; Partial oxidation; Rhodium; Hydrotalcite; Magnesium; Aluminum; Solid solution; Neutron diffraction; Synthesis gas; CO; H_2

1. Introduction

The use of natural gas as a raw material is a future goal of strategic importance. The economy of its utilisation is related to the activation of methane [1]. Indeed, the direct processes to C_2 and methanol are not attractive due to the low yields obtained to date and the indirect processes to syngas are still expensive and do not permit intensive methane exploitation [2,3]. Considerable academic and industrial research has been focused on the catalytic partial oxidation of methane as an interesting process to convert methane into liquid products. The reaction has been well known since Prettre et al. reported the activity of a Ni-based catalyst [4]; nevertheless, the discovery that high methane conversion and high synthesis gas selectivity would be possible at low residence time enhanced interest in the partial oxidation of methane [5,6]. Many aspects of this reaction have not yet been clarified, but it is clear that application of the process requires improvements in the temperature control, to avoid homogeneous reactions at high pressure [7,8], and an increase in the catalyst durability, to avoid sintering of the active metal. An innovative strategy able to improve the catalyst stability is based on the use of noble metal catalysts derived by reduction of crystalline oxide precursors [9,10]. The metal–support interaction in this case is expected to be stronger than that obtainable by the usual impregnation or deposition methods. The thermal evolution of noble metal catalysts with high activity prepared using hydrotalcite-type precursors has recently been reported [10,11]. The thermal decomposition of these catalysts led to the formation of defective structures. There is a need, therefore, to conduct further studies on these systems with a view to ascertain the relationship between structure before and after reduction and reactivity. The work reported here was focused on analysing the distribution of the noble metal at each of the steps that lead to the final catalyst, using a model catalyst (Rh/Al/Mg 5/24/71 a.r.). Understanding of the position of Rh and full characterisation of the material are a step towards being able to tailor new catalysts active in the partial oxidation of methane. In each stage of the thermal treatment of the material the appropriate technique was used to evidence the Rh position and the main characteristics of the materials.

* Corresponding author.
E-mail address: basile@ms.fci.unibo.it (F. Basile).

0021-9517/03/$ – see front matter
doi:10.1016/S0021-9517(03)00021-6

2. Experimental

The catalyst (Rh-5) was obtained by calcination and reduction of a hydrotalcite-type (HT) precursor. The HT precursor, formula $(Rh^{3+}_{0.05}Al^{3+}_{0.24}Mg^{2+}_{0.71}(OH)_2)(CO_3)^{2-}_{0.145} \cdot mH_2O$, was prepared by coprecipitation at constant pH (10.0 ± 0.1): a solution containing the nitrate salts of the metal ions was added to a solution containing a slight excess of carbonate. The pH was kept constant by dropwise NaOH addition. The addition of the cation solution was carried out in 20 min and then the precipitates were kept in suspension under stirring at 60 °C for 40 min, filtered, and washed with distilled water until a Na_2O content lower than 0.02 wt% was obtained. Two chemical analyses were carried out on the precipitate. Atomic absorption spectroscopy was used for the Mg and Al analyses and Rh was analysed using a UV–visible spectrophotometer [12,13]. The first analysis was carried out on the precipitate obtained after half of the cation solution had been added, the second on the final precipitate. The precipitate was dried overnight at 90 °C, calcined at 900 °C, and reduced at 750 °C in an equimolar H_2/N_2 feed of 7 l/h [10,11]. The cationic ratio of the surface precursor was determined by XPS VG 8 vacuum generators (ESCA 3) operating under ultra vacuum 5×10^{-7} Pa, using the K_α radiation emission of Mg (at constant energy per pass: 1253.6 eV, 20 mA), since with Al irradiation overlapping occurred between the 3*d* peak of Rh and an Auger peak of Mg. The XPS cationic ratio was calculated using the sensitivity factors reported by Wagner et al. [14], data for the Al_{2p} orbital, an average of the data obtained with the Mg_{2s} and Mg_{2p} orbitals, and the sum of the two $Rh_{3d(3/2+5/2)}$ unresolved peaks. The XRD powder analyses were carried out using a Philips PW1050/81 diffractometer equipped with a graphite monochromator in the diffracted beam and controlled by a PW1710 unit ($\lambda = 0.15418$ nm). A 2Θ range from 10° to 80° was investigated at a scanning speed of 70 °/h.

The TPR analysis was carried out with an H_2/Ar 4/96 v/v mixture (total flow rate 50 ml/min) with the temperature ranging from 30 to 980 °C using a ramp of 15 °C/min. The surface areas were determined by N_2 absorption using a Carlo Erba Sorpty Model 1700. The metal particle distribution of the Rh after reduction was measured using a TOPCON EM002K HRTEM operating at 200 kV. The sample was prepared by suspending a small amount of powder in an alcohol solution and depositing it on a carbon grid. The distribution was determined with a zoom of 500,000× of areas containing 100 particles. The analysis of the carbon content was carried out by the Centre National de la Recherche Scientifique-Service National d'Analyse (France) before and after reaction.

2.1. Catalytic tests

The catalytic tests were carried out under autothermal conditions, after the ignition of the reaction by means of a thermal gun, and under isothermal conditions using an oven at 750 °C, feeding three gas mixtures (CH_4/O_2/He = 2/1/4, 2/1/20, and 2/1/2 v/v) and using a quartz reactor (i.d. 8 mm) filled with 0.2 g and 0.075 mg of catalyst, in order to vary the residence time from 24 to 7.2 ms and from 9 to 1 ms, respectively. The lengths of the catalytic bed were 9 and 3 mm, respectively. The gas phase temperature was measured by a moveable chromel–alumel thermocouple inserted in a quartz wire inside the catalytic bed. The reaction products were analysed on line, after water condensation, by two gas chromatographs equipped with HWD and Carbosieve SII columns, with He as the carrier gas for the analysis of CH_4, O_2, CO, and CO_2 and N_2 as the carrier gas for the H_2 analysis.

The surface temperature was measured with IR thermography equipment (AGEMA) collecting emitted radiation with λ in the range 2–5 mm. The IR camera was equipped with two zooms to improve the spatial resolution on the catalyst surface. The vertical thermal profile was obtained by plotting the maximum temperature of the horizontal lines drawn on the thermography images. The catalyst have been compared with two commercial catalysts containing respectively 1.0 wt% of Rh on α-Al_2O_3 (Snamprogetti) and 5.0 wt% of Rh on γ-Al_2O_3 (Engelhard).

3. Results and discussion

3.1. Precursor structure

In order to understand the distribution of the Rh inside the hydrotalcite-type precursor and the evolution of the material during preparation, the catalyst Rh/Al/Mg 5/24/71 a.r. was studied. The precursors was prepared by coprecipitation and accurate chemical analysis was carried out to determine the chemical composition at different stages of the preparation. The chemical analysis of the mother liquid did not show the presence of Mg, Al, and Rh residues, indicating, therefore, quantitative precipitation. Furthermore, the analysis of the cations contained in the precipitate at different precipitation times (half precipitation, final precipitation) showed no significant differences (Table 1), giving the same bulk composition and indicating simultaneous precipitation of the cations due to the high supersaturation regime. Both the samples, obtained at different precipitation times, show the XRD pattern (Fig. 1) of a hydrotalcite-type precursor with an increase in crystallinity due to the aging of the precipitate

Table 1
Bulk surface and intermediate composition of the precursor prepared with the nominal cationic ratio Rh/Mg/Al 5/71/24 (a.r.)

Cations composition	Nominal	Precipitate	Surface	After half cation addition
Mg (atomic ratio)	71.0	70.8	71.4	70.6
Al (atomic ratio)	24.0	24.4	24.0	24.5
Rh (atomic ratio)	5.0	4.8	4.6	4.9

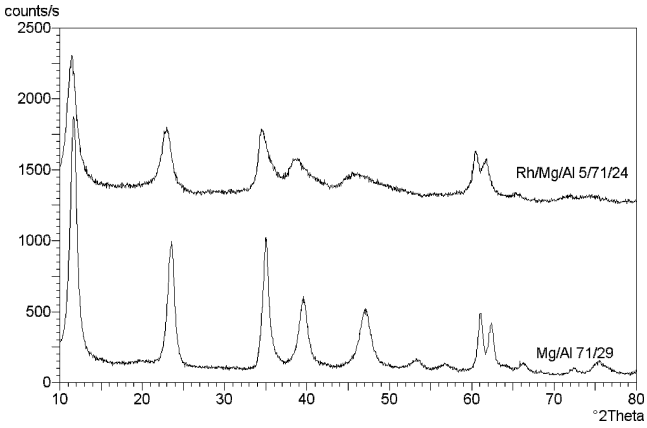

Fig. 1. XRD patterns of the Rh/Mg/Al 5/71/24 a.r. precursor compared with the Mg/Al 71/29 a.r. precursor.

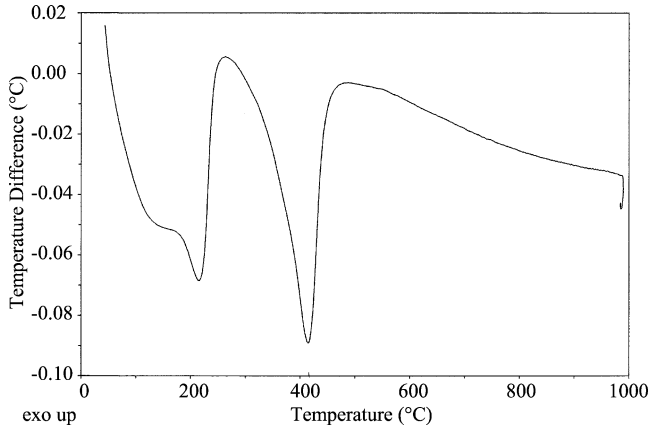

Fig. 2. DTA of the Rh/Mg/Al 5/71/24 a.r. precursor (temperature ramp 10 °/min).

in the solution. The crystallinity of the final precursor was sufficient to allow determination of the cell parameters. The cell parameters are modified by the presence of the transition metal cation Rh^{3+} with respect to a reference sample containing only Mg and Al. In particular, the *c* parameter of the Rh samples is higher due to the presence of Rh^{3+}, which has a smaller charge density than Al^{3+}. The *a* parameter of the HT precursor is slightly higher due to the larger anionic radius of Rh^{3+} as compared with that of Al^{3+}. To confirm the presence of Rh in the HT structure, with respect to an amorphous side phase possibly present, XPS analysis was carried out on the precursor. The surface composition, reported in Table 1, is compared with the bulk composition in terms of M/Al, confirming the homogeneity of the precursor. The variation, less than 10%, is close to the experimental error, confirming the presence of Rh in a solid solution with the Al and Mg in the HT structure. Calculated XRD patterns of Mg/Al and Rh/Mg/Al HT samples show very similar diffraction intensities of the main peaks for 5% Rh content. This means that it is not possible to carry out a Rietveld analysis to confirm the insertion of Rh atoms into the HT crystalline structure. In any case the results obtained clearly indicate the formation of an Rh/Mg/Al HT precursor.

3.2. Mixed oxide phase structure

The DTA analysis of the precursor shows the typical decomposition pattern of an HT structure, with loss of the interlayer H_2O at 240 °C and the second simultaneous loss of H_2O from the hydroxyl group of the layer, and CO_2 at 430 °C (Fig. 2), that indicate decomposition of the HT with formation of a mixed oxide phase. In order to analyse the structure changes and the location of the Rh in the sample in an intermediate temperature range far from the decomposition temperature of the HT precursor and from the rearrangement of the mixed oxide structure (750 °C) we chose a temperature of 650 °C.

When calcined at 650 °C, the HT structure decomposes, giving a defective mixed oxide phase. To study the main features of such a structure, XRD and neutron diffraction analyses were carried out. The two techniques are complementary and indispensable to the study of the oxide systems discussed herein. For instance, determination of the occupancy factors of Mg and Al atoms from X-ray data is hindered by the closeness of the X-ray scattering of both elements. The two have significantly different neutron scattering factors. On the other hand, it is difficult to identify the sitting of the transition metals exclusively from neutron data because of the low substitution rate. The enormous differences between the X-ray scattering lengths of the transition metals investigated herein and those of Mg and Al atoms allow refinement of data based on the sitting of a small percentage of the heavier metal.

The location and amount of the transition metals was determined from the full pattern refinement of both X-ray and neutron data.

Previous studies demonstrated that although mixed oxides obtained from magnesium containing HT precursors show diffraction patterns similar to those of MgO-type phases, their lattices are far from an ideal "rock-salt" phase. The broadening and shift of the reflection at $2\theta \cong 37°$ detectable in the X-ray diffraction patterns alludes to the presence of a distorted MgO-type phase [15–17]. Therefore, a more flexible spinel-like structure was adopted to model the MgO-type phase [15–17].

MgO and stoichiometric spinel have the same framework of oxygen atoms, which differ essentially in two features: (i) the *a* unit cell parameter of the spinel cell axis is almost twice that of the oxide one (8.083 Å for $MgAl_2O_4$ compared to 4.213 Å for MgO) [18], and (ii) the location of the cations and the degree of filling of the cavities defined by the oxygen atoms vary. In the spinel unit cell there are 32 oxygen atoms defining 32 octahedral and 64 tetrahedral interstices. In a stoichiometric $MgAl_2O_4$ spinel, only one-eighth of the tetrahedral (crystallographic site 8a) and one-half of the octahedral cavities (site 16d) are occupied [19–21].

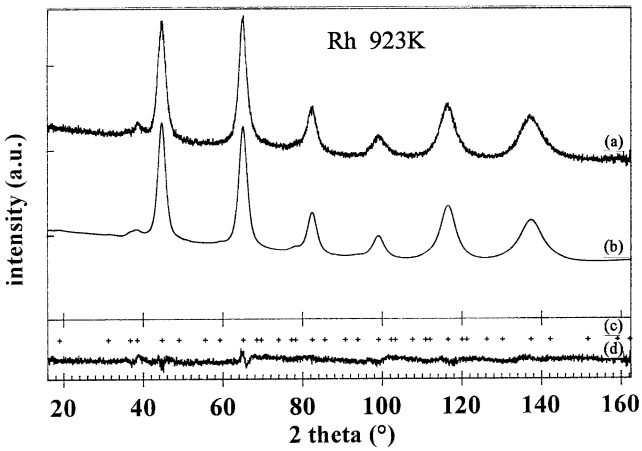

Fig. 3. Results of the combined Rietveld analysis using XRD and neutron diffraction for the Rh/Mg/Al 5/71/24 a.r. sample calcined at 650 °C: (a) observed profile, (b) calculated neutron powder profile, (c) reflection position markers, and (d) difference profile.

Therefore the spinel structure has many empty sites in which the ions can be accommodated.

The MgO unit cell (space group F$m3m$ No. 225) contains four oxygen atoms and four crystallographically equivalent metal atoms in octahedral coordination, giving rise to the so-called "rock-salt" type structure. This lattice can be described using a supercell with a lattice parameter twice that of the oxide and the scaled down co-ordinates reported for the stoichiometric spinel space group, F$d3m$ (No. 227) [20,22]. The volume of the oxide supercell is eight times that of the original cell and contains 32 oxygen atoms and 32 cations that fill all the octahedrally coordinated positions. Due to the F$d3m$ space group symmetry rules [22], the octahedral sites are nonequivalent and are identified as 16c and 16d. In a stoichiometric $MgAl_2O_4$, Al atoms occupy the 16d sites; the 16c sites are empty, while the Mg atoms occupy the tetrahedrally coordinated positions (sites 8a). The 8a sites are empty in a "rock-salt" structure such as MgO. In other spinels, the distribution of the cations in the cavities may be different [23–25]. Nonstoichiometric spinels show structures intermediate between the spinel and "rock-salt" types [15–17].

The X-ray and neutron diffraction patterns of the sample calcined at 650 °C are shown in Fig. 3 while the distribution of the metal cations inside the different crystallographic positions derived from the refinements is reported in Table 2. The refined data clarify that the main deviation of this structure from ideality is the presence of 30% of the Mg ions in the tetrahedral 8a sites typical of a spinel-type structure, while the rest are spread throughout the 16c and 16d sites, compensated for by the presence of the trivalent cations (Al and Rh) exclusively in the octahedral 16d sites, in analogy with the spinel-type structure. Furthermore, the 16c sites are not completely filled, very likely with a lack of cations in correspondence with the 8a filled sites. These sites are in fact due to the closeness of the cations and the prevailing repulsive forces.

The results of the refined a parameter show that the cell is smaller than the MgO supercell (twice that of MgO, i.e., 8.426 Å) [18]. This is in agreement with the cations present and positions of the cations, as can be expected from the presence of the cations with radii smaller (Rh^{3+} 0.80, Al^{3+} 0.67 Å) [26] than that of Mg (0.86 Å) and the evolution towards a spinel-like structure with a smaller a parameter ($a = 8.085$ Å [20] for a stoichiometric Mg/Al spinel).

In the samples calcined at 900 °C (Fig. 4), a cubic spinel type oxide phase is observed along with a MgO-type phase similar to that detected for the sample calcined at 650 °C. No separate Rh-phase is observed after calcination at 900 °C, indicating that the solubility of Rh in the mixed oxide phases is complete. On the basis of these results, the refinement was conducted using two spinel structures with different unit cell parameters allowing the possibility of having cations in the

Table 2
The detected phases, refined structural parameters, and agreement indices R_p, R_{wp} for the sample calcined at 650 °C (e.s.d. in parentheses)

	Detected phases		
	MgO[a] (650 °C)	MgO[a] (900 °C)	Spinel (900 °C)
a (Å)[b]	8.3833(8)	8.4212(3)	8.1379(4)
x[c]	0.2496(5)	0.2526(3)	0.2604(3)
Position[d]	16c 16d 8a	16c 16d 8a	16c 16d 8a
O.F.(Mg)	0.80(3) 0.26(5) 0.27(2)	0.92(4) 0.47(3) 0.16(3)	0.11(2) 1.00(3)
O.F.(Al)	0.42(3)	0.26(3)	0.77(3)
O.F.(Rh)	0.091(6)	0.076(6)	0.112(5)
Proposed chemical formula[e]	$Mg_{0.60}Al_{0.21}Rh_{0.047}O$	$Mg_{0.73}Al_{0.13}Rh_{0.038}O$	$Mg_{1.3}Al_{1.6}Rh_{0.224}O_4$
R_p	2.1	2.4	2.2
R_{wp}	2.6	3.0	2.7

[a] MgO = MgO-type phase.
[b] Refined value relative to the mixed oxide supercell (spinel-type cell). Divide by 2 in order to compare with MgO lattice type.
[c] Oxygen fractional coordinate.
[d] Cation presence was tested also in the 8b site but the O.F. were so close to zero that this site was considered empty in the final cycles. The occupation factors are normalised to unity.
[e] In the unit cell are contained 32 formula units indicated for MgO-type phase and 8 for spinel-type phase.

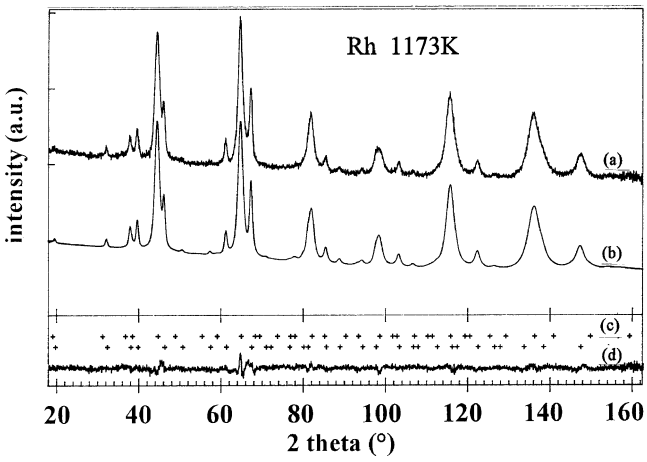

Fig. 4. Results of the combined Rietveld analysis using XRD and neutron diffraction for the Rh/Mg/Al 5/71/24 a.r. sample calcined at 900 °C: (a) observed profile, (b) calculated neutron powder profile, (c) reflection position markers, and (d) difference profile.

octahedral 16c, 16d and tetrahedral 8a, 8b sites (Table 2). The MgO type phase of the samples calcined at 900 °C shows lower Al and Rh contents, although some Rh is still present in this phase, a lower occupancy of the 8a sites, and further filling of the 16d sites. Indeed segregation of the spinel phase leads to the rearrangement of the Mg/Al atoms inside the MgO-type phase at 900 °C, which shows a distribution of atoms much closer to a "rock-salt" structure than in the 650 °C sample. This is also shown by the increase in the cell parameters that have values close to that of ideal MgO. In contrast, the spinel-like phase is characterised by the presence of some Mg (20%) in octahedral position. The presence of Mg in octahedral position is not balanced by the presence of trivalent cations in tetrahedral positions (inverse spinel); therefore, it is probably balanced by the presence of oxygen vacancies. The cell parameters in this case are larger than those of $MgAl_2O_4$ because of the presence of Rh which partially substitutes for Al in the octahedral 16d sites.

From the reported data it is evident that Rh is present in both the spinel- and MgO-type phases. The relative % of Rh present in the spinel-type phase is higher than that present in the oxide phase, i.e., the solubility of the transition element in the spinel-type phase is considerably higher than in the MgO-type oxide. Nevertheless, the absolute atom % distribution shown in Table 3 (the product of the proportion of the element substitution in a particular phase and the amount of the phase in the sample) shows that the Rh is more present in the oxide phase. In particular, its distribution for each phase is the following: 41% of the Rh atoms in the spinel and 59% in the MgO-type phase, considering that the amount of the MgO-type phase is much higher than the spinel-type phase. Finally an interesting consideration can be made comparing the relative distribution of Al and Rh in the MgO phase (0.33 and 0.67, respectively), demonstrating that the affinity of Rh^{3+} for the MgO phase is double of that of Al^{3+} (ionic radii 0.80 and 0.67 Å, respectively).

Table 3
Phase composition and distribution of the cations between the different crystalline phases obtained after calcination of the HT precursor (e.s.d. 2% of the values)

	Rh (923 K)	Rh (1173 K)
MgO–S (%wt)[a]	100–0	69–31
Spinel fraction[b]	0	32
M_{MgO}–M_{spin} (atom%)[c]	100–0	59–41

[a] MgO = MgO-type phase; S = spinel-type phase; M = Rh, Ir, or Ru.
[b] Ratio between the spinel and the total mixed oxides: S/(MgO + S) as mol%.
[c] Distribution % of the transition metal atoms between the one (923 K) or two phases (1173 K).

3.3. Reducibility of rhodium

The HT calcined at 650 and 900 °C was characterised by TPR experiments to obtain information on the degree of reducibility and the temperature at which the process occurs. Three main peaks are clearly present at both calcination temperatures (Fig. 5). The experiments show that the temperature of the first reduction peak does not depend on the calcination temperature and is close to 410 °C while the area of the peak increases with increasing calcination temperature. The results of the diffraction refinement and the high temperature at which the first reduction occurs indicate that the reduction is not due to an amorphous Rh_2O_3 phase. The TPR of the sample calcined at 900 °C shows that the two peaks at high temperatures are shifted towards higher temperature because of the formation of more crystalline and fewer defect phases.

The high reduction temperature of the Rh is due to its insertion into the mixed oxide phases. The TPR studies allow determination of the best reduction conditions. Total Rh reduction was obtained at 750 °C in an H_2/N_2 atmosphere for 4 h. The catalyst was analysed by TEM before the catalytic tests. The image of the samples with a lower zoom factor shows that the Rh is homogeneously distributed on a Mg/Al oxide matrix. The grain of the matrix are constituted by nanodomains (Figs. 6, and 7). Differentiation between the MgO-type and spinel matrix is not possible using EDAX micoranalysis. Increasing the zoom factor makes it possible

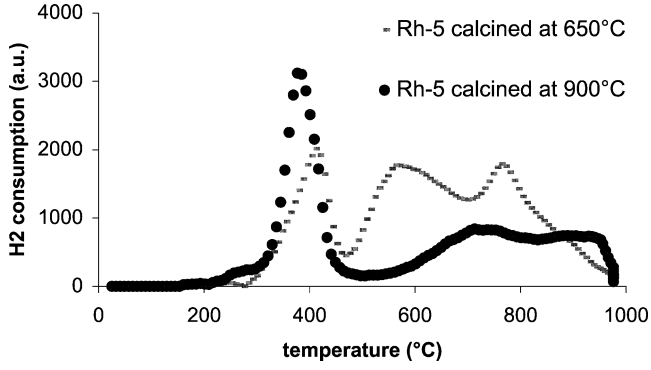

Fig. 5. TPR from 30 to 976 °C (10°/min) on 50 mg of the Rh/Mg/Al 5/71/24 a.r. sample calcined at 650 and 900 °C.

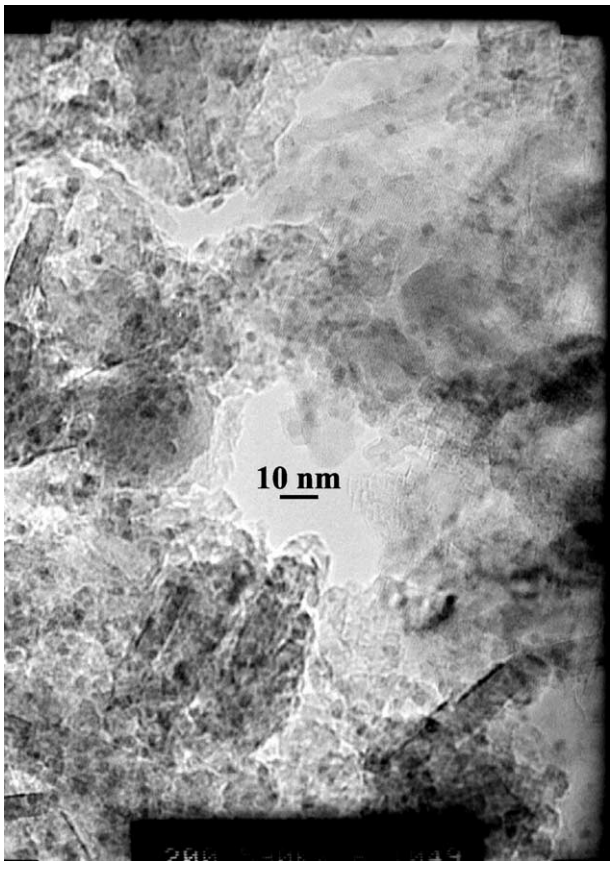

Fig. 6. TEM image (200, 000×) of the Rh-5 after calcination at 900 °C and reduction at 750 °C.

to see the atom columns and the crystalline plane of the oxide matrix together with an homogenous distribution of the Rh (Fig. 7). Nevertheless, even using a high zoom factor, the different MgO and spinel-type domains are not clearly separated and the only features distinguishable are those where the columns of atoms are visible. The EDAX analysis, notwithstanding the use of the smallest spot available, was not able to isolate parts of the sample with compositions typical of MgO and spinel since the crystallites are not separated and the domains are smaller than the spot (10 nm). Investigation of different zones indicated that the metal particles are surrounded and decorated by the oxide matrix which ensures a strong interaction with the metal. Nevertheless the morphology of the sample and the Rh distribution seem to be very homogeneous. Fig. 8 shows the distribution of the Rh particle dimensions collected on different zones. The distribution reported for more than 200 measured particles is very narrow and the average dimension is close to 2 nm.

3.4. Catalytic activity

The catalyst was tested in the partial oxidation of methane and some of the results have been reported previously [27,28]. Interesting results were obtained in several reaction conditions with varying amounts of catalyst, heat delivery, and

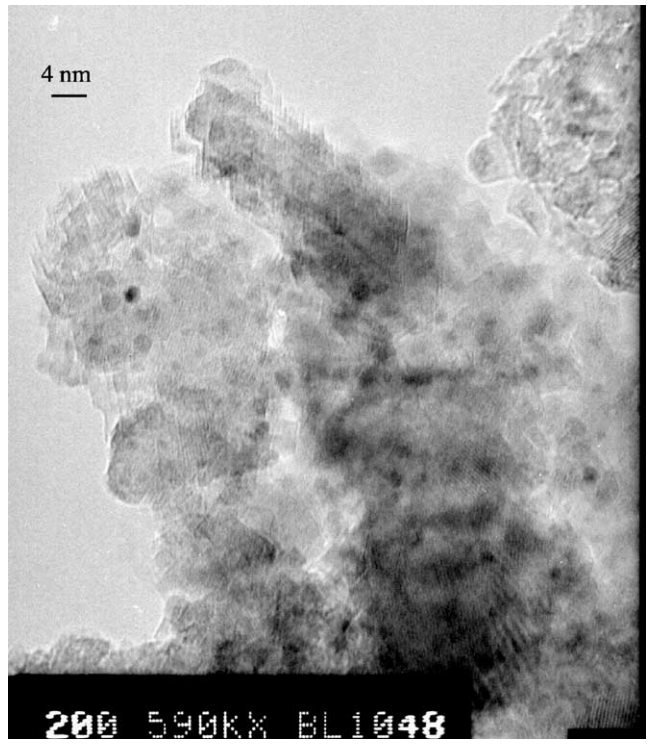

Fig. 7. TEM image (530, 000×) of the Rh-5 after calcination at 900 °C and reduction at 750 °C.

dilution of the feed. The catalyst has a light-off temperature of 260 °C. Over the entire range of conditions investigated the methane conversion and synthesis gas selectivity were close to those predicted for thermodynamic equilibrium. The methane conversion and syngas selectivity were very high during the isothermal conditions test (T oven 750 °C, $CH_4/O_2/He = 2/1/4$ v/v, residence time 1.8 ms; conversion of $CH_4 = 93\%$, selectivity of CO and H_2 94 and 92%, respectively). Notwithstanding the high dispersion due to the small dimensions of the catalytic bed (6 mm i.d., 3 mm height), the test carried out under autothermal conditions showed high activity, with total oxygen conversion and a residence time of 1 ms (Table 4). The increase of the catalytic performances by decreasing the residence time is due to an increase of the temperature as revealed by an in-

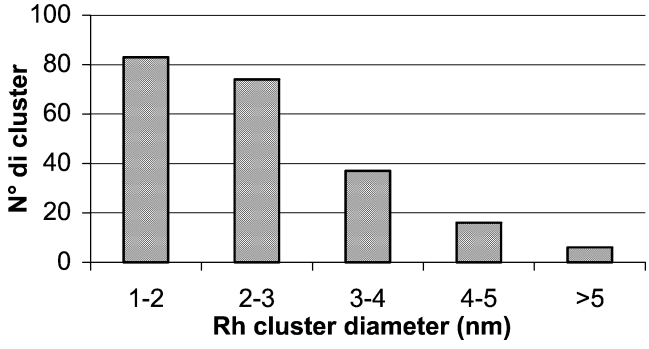

Fig. 8. Particle size distribution of Rh for the Rh-5 catalyst after calcination at 900 °C and reduction at 750 °C.

Table 4
Catalytic data under autothermal conditions ($CH_4/O_2/He = 2/1/4$ v/v; catalyst amount = 0.05 g)

Residence time (ms)	Conv CH_4 (%)	Sel CO (%)	Sel H_2 (%)	T_{max} surface (°C)
8.6	47.6	52.7	63.1	790
5.7	55.8	69.3	72.6	863
2.9	66.3	83.0	80.6	952
2.0	68.9	86.0	81.6	967
1.4	71.1	87.2	81.6	978
0.9	72.4	88.4	82.0	984

crease of the maximum temperature reported in the graph and by the enlargement of the hot zone shown for a residence time of 1.8 ms (Fig. 9). The same results have been reported mainly for monolith catalyst or gauze Pt/Rh catalysts where the heat diffusion is much more favourable [29–31]. A comparison among the present catalyst and commercial Rh catalysts can help to understand the activity of this catalyst and was carried out using two different samples: a catalyst containing 1% of Rh supported on α-Al_2O_3 and a catalyst containing a 5% of Rh supported on γ-Al_2O_3. The comparison was carried out under autothermal conditions at very low residence time (1 ms) and in isothermal conditions with an oven temperature of 750 °C and a diluted gas mixture ($CH_4/O_2/He = 2/1/20$ v/v), to limit the effect of the temperature increase (Table 5). Under adiabatic conditions the reaction is far from thermodynamic equilibrium and all the catalysts except the one prepared from HT precursor show partial conversion of oxygen. The oxygen leaching decreases with the increase of the active sites and it is not present for the Rh5 prepared from HT precursor. The isothermal conditions flatten the differences among the catalysts and the results are close to thermodynamic equilibrium. In the present case the high activity is due to the high surface area, which allows homogeneous dispersion of high amounts of Rh (10.6 wt.%). Even though the high activity of a catalyst with such a high amount of Rh may not be surprising, much more surprising is the stability of this catalyst towards sintering. In fact, the high amount of Rh should have favoured sintering. Experimental results after 50 h of tests during partial oxidation of methane in autothermal conditions (surface temperature at the beginning of the bed ≈ 965 °C, gas temperature at the exit of the bed ≈ 680 °C) (Fig. 9) and 50 h of tests during isothermal conditions (gas temperature 930 °C) still shows a very high dispersion of the Rh (HRTEM image). Comparison of the Rh particle size distribution of this

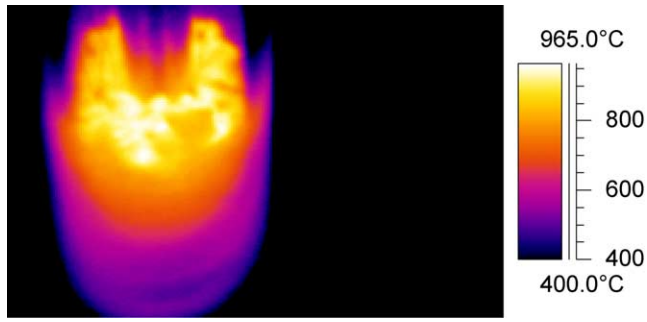

Fig. 9. IR thermography of the top catalyst bed measured under autothermal conditions ($CH_4/O_2/He = 2/1/4$ v/v, residence time = 1.8 ms, catalyst amount = 0.05 g).

catalyst before and after the reaction using HRTEM does not show any difference, confirming the high stability of this catalyst, which may be attributed to the interaction between metal and support [32] produced by the coprecipitation of Rh in an HT precursor and the presence of MgO and spinel phase as inert matrix [33]. The analysis of the carbon content in the samples before and after reaction (after 100 h of time on stream) shows an amount of 0.81% and 0.83% for the samples calcined at 900 °C and for the sample used, respectively. The constant amount of carbon demonstrate that no carbon accumulation is occurring during 100 h of reaction. Furthermore, since the particles dimension distribution is unchanged it is clear that this time does not correspond to an induction period. The presence of a certain amount of carbon also in the calcined sample is due to the presence of carbonate trapped in the structure and/or readsorbed as CO_2 from the atmosphere to give traces of HT reconstruction.

4. Conclusions

Development of the catalytic partial oxidation of methane on industrial scale requires the development of an active and stable catalyst prepared by a bulk technique such as those obtained by HT precursors. The catalyst preparation was studied in each reaction step to ensure high reproducibility and to increase the knowledge and control of the structural properties of the final catalyst. The study of the preparation step demonstrated that the Rh is inserted into the precursor by coprecipitation. Furthermore XPS analysis confirms that the cations are homogeneously distributed between bulk and surface. The calcination step induces decomposition of the HT precursor and formation of a defective mixed oxide

Table 5
Comparison of the catalytic activity of Rh catalysts in autothermal conditions and under diluted conditions T_{oven} = 750 °C, $CH_4/O_2/He = 2/1/20$ v/v, τ = 1 ms

	Diluted conditions T_{oven} 750 °C			Autothermal conditions			
Sample	Conv CH_4	Sel CO	Sel H_2	Conv CH_4	Sel CO	Sel H_2	Conv O_2
Rh-5 HT	94.6	96.2	91.5	72.4	88.4	82.0	100.0
Rh-5 α-Al_2O_3	93.2	95.2	89.8	68.5	86.2	78.5	98.1
Rh-1 γ-Al_2O_3	93.4	95.0	90.1	62.2	86.3	75.6	94.5

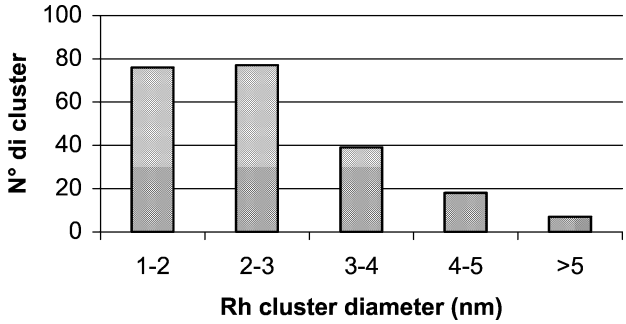

Fig. 10. Particle size distribution of Rh for the Rh-5 catalyst after 100 h of time on stream in partial oxidation of methane (50 h of autothermal and 50 h of isothermal conditions).

phase with a structure similar to that of MgO. The defects are related to the presence of some Mg^{2+} cations in tetrahedral positions and of course to a number of cation vacancies due to the presence of M^{3+} (Al^{3+} and Rh^{3+}) in octahedral positions. At 900 °C the rearrangement of the structure forms a more ideal MgO phase which still has some trivalent cations in its structure and a spinel phase. The solubility of Rh in the spinel phase is higher than that in the MgO phase, but being the latter more abundant, the total amount of Rh is distributed 41% in the spinel type phase and 59% in the MgO. The TPR analysis shows three distinct peaks due to the reduction of Rh^{3+} to Rh^0. After reduction the HRTEM evidenced still an high interconnection between matrix and metal particles of size 2 nm with a narrow size distribution stable also after catalytic tests. Notwithstanding the severe reduction procedure and the high metal loading the prepared material shows very disperse metal particles on the surface (2 nm). As a consequence, the catalytic activity is very high also at very low residence time (1 ms) in both autothermal and isothermal conditions. Finally, the metal support interaction allows a stable dispersion also after 100 h time on stream (Fig. 10). The dispersion of the metal is unchanged before and after reaction. In conclusion, the material derived from a hydrotalcite-type precursor allows control of the metal position in each stage of the preparation, giving rise to a very interesting catalyst for high-temperature applications, due to its high dispersion and stability with time on stream.

Acknowledgments

Financial support from the Ministero dell' Istruzione, dell' Universitá e della Ricerca (MIUR, Rome, Italy) is gratefully acknowledged.

References

[1] J.P. Lange, Catal. Today 64 (2001) 3.
[2] M.J. Brown, N.D. Parkyns, Catal. Today 8 (1991) 305.
[3] J.M. Fox, Catal. Rev. -Sci. Eng. 35 (1993) 169.
[4] M. Prettre, Ch. Eichner, M. Perrin, Trans. Faraday Soc. 43 (1946) 355.
[5] D.A. Hickman, L.D. Schmidt, J. Catal. 138 (1992) 267.
[6] V.R. Choudhary, A.S. Mamman, S.D. Sansare, Angew. Chem. Int. Ed. Engl. 31 (1992) 1189.
[7] L. Basini, K. Aasberg-Petersen, A. Guarinoni, M. Østberg, Catal. Today 64 (2001) 9.
[8] L.D. Schmidt, O. Deutschmann, C.T. Goralsky Jr., in: A. Parmaliana, et al. (Eds.), Natural Gas Conversion V, in: Studies in Surface Science and Catalysis, Vol. 119, Elsevier, Amsterdam, 1998, p. 685.
[9] H. Provendier, C. Petit, C. Estournès, S. Lins, A. Kiennemann, Appl. Catal. A 180 (1999) 163.
[10] F. Basile, L. Basini, G. Fornasari, M. Gazzano, E. Poluzzi, F. Trifirò, A. Vaccari, in: B. Delmon, et al. (Eds.), Preparation of Catalysts VII, in: Studies in Surface Science and Catalysis, Vol. 118, Elsevier, Amsterdam, 1998, p. 31.
[11] L. Basini, G. Fornasari, F. Trifirò, A. Vaccari, Eur. Pat. Appl. 101,059, 1996.
[12] A. Vogel, Textbook of Quantitative Inorganic Analysis, Longman, London, 1978.
[13] G. Charlot, Chimie Analytique Quantitative, Masson, Paris, 1974, p. 490.
[14] C.D. Wagner, L.E. Davis, M.V. Zeller, J.A. Taylor, R.M. Raymond, L.H. Gale, Surf. Interface Anal. 3 (1981) 211.
[15] B. Rebours, J.B. d'Espinose de la Caillerie, O. Clause, J. Am. Chem. Soc. 116 (1994) 1707.
[16] M. Gazzano, W. Kagunya, D. Matteuzzi, A. Vaccari, J. Phys. Chem. B 101 (1997) 4514.
[17] M. Bellotto, B. Rebours, O. Clause, J. Lynch, D. Bazin, E. Elkaim, J. Phys. Chem. 100 (1996) 8535.
[18] Files 4-829 (MgO), 21-1152 ($MgAl_2O_4$), International Center for Diffraction Data, Newtown Square, PA, USA.
[19] A.F. Wells, Structural Inorganic Chemistry, Oxford Univ. Press, Oxford, 1984, p. 592.
[20] R.W.G. Wyckoff, in: Crystal Structures, Vol. 4, Interscience, New York, 1968, p. 76.
[21] P. Fischer, Z. Krist. 124 (1967) 275.
[22] International Tables for X-ray Crystallography, Vol. I, Kynoch Press, Birmingham, 1974.
[23] R.C. Peterson, G.A. Lager, R.L. Hitterman, Am. Mineral. 76 (1991) 1455.
[24] W.L. Smith, A.D. Hobson, Acta Crystallogr. Sect. B 29 (1973) 362.
[25] H. Berg, E.M. Kelder, J.O. Thomas, J. Mater. Chem. 9 (1999) 427.
[26] R.D. Shannon, Acta Crystallogr. Sect. A 32 (1976) 751.
[27] F. Basile, L. Basini, G. Fornasari, M. Gazzano, F. Trifirò, A. Vaccari, Chem. Commun. (1996) 2435.
[28] F. Basile, G. Fornasari, F. Trifirò, A. Vaccari, Catal. Today 64 (2001) 21.
[29] M. Fathi, K. Heitnes Hofstad, T. Sperle, O.A. Rokstad, A. Holmen, Catal. Today 42 (1998) 205.
[30] P.M. Witt, L.D. Schmidt, J. Catal. 163 (1996) 465.
[31] J.C. Slaa, R.J. Berger, G.B. Marin, Catal. Lett. 43 (1997) 63.
[32] H. Knözinger, E. Taglauer, in: G. Ertl, et al. (Eds.), Handbook of Heterogeneous Catalysis, Vol. 1, VCH, Weinheim, 1997, p. 222.
[33] E. Ruckenstein, H.Y. Wank, Appl. Catal. A Gen. 198 (2000) 33.